



## B

layer. The classical SD model can be written as

$$J_w = \frac{D_{wm} C_{wm} \bar{V}_w}{R_g T \delta} (\Delta P - \Delta \pi) = A (\Delta P - \Delta \pi) \quad (1)$$

The membrane water diffusivity,  $D_{wm}$ , and membrane water concentration,  $C_{wm}$ , and so the water permeability,  $A$ , are assumed to be constant for a particular temperature. However, in the case of dilute organics (with negligible osmotic pressure), this model, on one hand, fails to predict flux behavior unless membrane–organic interaction terms can be included. On the other hand, organic separation (solute flux) prediction with an extended SD model by incorporation of an additional pressure-induced solute transport parameter has been reported.<sup>18</sup> Although this model adequately described negative rejection behavior observed by phenol on cellulose acetate, it does not address substantial decreases in water flux found for some dilute organic systems.

In addition to solution–diffusion-based models, pore models also provide RO membrane transport behavior. One of the early models proposed was the Kimura–Sourirajan analysis (KSA) which defines the membrane as a barrier layer with preferential sorption for the water or repulsion of solutes.<sup>19,20</sup> The solute permeability coefficient has also been correlated with various membrane constants and solute Taft parameters which measure steric and polar behavior.<sup>8,15,21,22</sup> For example, Dickson et al.<sup>15</sup> verified the model with FT-30 membranes for simple binary systems such as dilute 2-propanol and *tert*-butanol. The finely-porous model (FPM) was first proposed by Merten<sup>23</sup> and in modified form by Johnsson and Boeson<sup>24</sup> which assumed viscous transport of water and diffusive and convective transport of solutes through the pores. Mehdizadeh and Dickson<sup>25</sup> reported the modification of the FPM model by correcting the solute material balance and the osmotic pressure effects and provided the mathematical techniques to find the optimum values of the 3–4 adjustable parameters. Niemi and Palosaari<sup>26</sup> applied the model to predict the separation of dilute ethanol and acetic acid streams. However, the use of the FPM model for highly interacting organics required a correction of the pore size value. A somewhat complicated but highly elegant pore model to account for organic separations is the surface force pore flow (SFPF) model which was first developed by Matsuura and Sourirajan.<sup>6</sup> Some of the assumptions include water transport by viscous flow, solute transport by convection and diffusion, transport determined by interaction forces and friction forces, and preferential sorption of water on the pore wall. The SFPF model has been extended to describe the performance of cellulose acetate RO membranes for the separation of dilute organics (interacting), but this required 5 adjustable parameters. The model was found to be reasonably consistent with literature data involving toluene, cumene, and *p*-chlorophenol.<sup>27</sup>

For charged NF or RO membranes, although the water flux can be calculated with eq 1, the prediction of ionized solute rejection will require the incorporation of both diffusion and charge repulsion (Donnan exclusion). The Nernst–Planck equation can be applied to these types of systems.<sup>28–30</sup> Application of this model requires determining the charge density by theory or ion-exchange capacity of the membrane, charge density as a function of pH, transport parameters for diffusion

and ion velocity, and distribution coefficients. Thus, on the basis of Donnan exclusion model, one would expect a strong dependency on organic separation with the degree of ionization of solute. This effect is further discussed in the NF section.

### Proposed Steady-State and Unsteady-State RO Models Involving Dilute Organic–Water Systems

Two types of models are formulated to describe the flux and separation behavior of organics that interact with polymer materials. One model is a modification of the SD model to include the effects of organic sorption/adsorption in the membrane. The second model is a diffusion–adsorption-based unsteady-state model. The models assume that transport and separation characteristics are determined by the membrane thin-skin barrier layer of the composite membranes. The formulated transport equations were solved numerically.

**(1) Modified Solution-Diffusion (MSD) Model (Steady-State Model).** The solution-diffusion model assumes that both water and solute transport across the membrane occurs by diffusion. For organics that can strongly sorb in the membrane, Rautenbach and Gröschl<sup>31–33</sup> pointed out that a more reasonable assumption would be that the total solute ( $C_m$ ) and water ( $C_{wm}$ ) concentration in the membrane is constant:

$$C_{tm} = C_m + C_{wm} \quad (2)$$

where  $C_{tm}$  is the total concentration in the membrane. This implies that there is a finite number of sites within the membrane that can be occupied by both the water and the solute. If this expression is substituted into eq 1, we get the following expression:

$$\begin{aligned} J_w &= \left( \frac{C_{tm} - C_m}{C_{tm}} \right) \frac{C_{tm} D_{wm} \bar{V}_w}{R_g T \delta} (\Delta P - \Delta \pi) \\ &= \left( 1 - \frac{C_m}{C_{tm}} \right) A^* (\Delta P - \Delta \pi) \end{aligned} \quad (3)$$

where  $A^*$  represents a new permeability constant and does not depend on the water concentration in the membrane but instead the total concentration in the membrane. Rautenbach and Gröschl<sup>31–33</sup> also showed that the quantity  $C_m/C_{tm}$  in eq 3 can be represented by a Langmuir type:

$$\frac{C_m}{C_{tm}} = \frac{b_0 C_F}{1 + b_0 C_F} \quad (4)$$

which, upon substitution in eq 3, results in

$$\begin{aligned} J_w &= \left( 1 - \frac{b_0 C_F}{1 + b_0 C_F} \right) A^* (\Delta P - \Delta \pi) = \\ &= \left( \frac{1}{1 + b_0 C_F} \right) A^* (\Delta P - \Delta \pi) \end{aligned} \quad (5)$$

Equation 5 indicates that the water flux through the membrane depends not only on the effective pressure driving force ( $\Delta P - \Delta \pi$ ) across the membrane but also on the solute feed concentration. In the presence of the concentration polarization  $C_F$  needs to be replaced by the wall concentration.

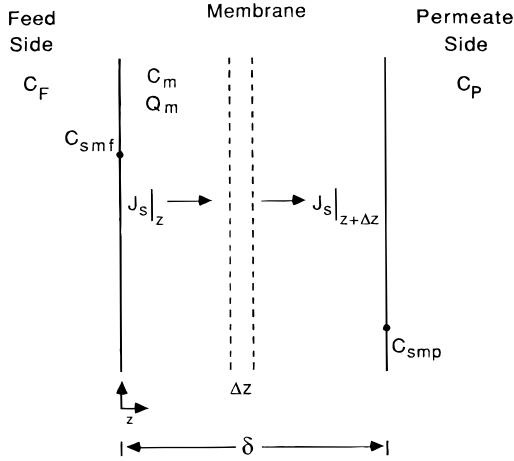


**Figure 1.** Membrane cross section depicting flux and solute partitioning.

For dilute solutions the solute transport can be described (as in the SD model) by solute diffusion across the membrane as

$$J_s = \frac{D_{sm}}{\delta} (C_{smf} - C_{smp}) \quad (6)$$

However, instead of a linear partition coefficient, as in the SD model, the partition is determined by a Langmuir isotherm like that used in the water flux expression:

$$C_{smf} = \frac{C_{tm} b_0 C_F}{1 + b_0 C_F} \quad (7)$$

$$C_{smp} = \frac{C_{tm} b_0 C_P}{1 + b_0 C_P} \quad (8)$$

which, when substituted in eq 6, results in

$$J_s = \frac{D_{sm} C_{tm}}{\delta} \left( \frac{b_0 C_F}{1 + b_0 C_F} - \frac{b_0 C_P}{1 + b_0 C_P} \right) = B^* \left( \frac{b_0 C_F}{1 + b_0 C_F} - \frac{b_0 C_P}{1 + b_0 C_P} \right) \quad (9)$$

where  $B^*$  represents a solute permeability constant.

Equations 5 and 9 represent the water and solute fluxes through the membrane for the modified solution-diffusion (MSD) model. An explicit form of eq 9 for solute flux that does not contain the permeate concentration can be easily obtained by substituting  $C_P = J_s/J_w$  and solving the resulting quadratic for  $J_s$ .

**(2) Diffusion-Adsorption (DA) Model (Unsteady-State Model).** The water and solute flux expressions developed for the MSD model represent steady-state fluxes across the membrane. The water fluxes usually reach steady state quickly and so are adequately described by eq 5. However, some solutes can adsorb in the membrane pores as these are transported across the membrane and, as a result, transient behavior is observed in the permeate concentration. A diffusion-adsorption (DA) model has been formulated below to describe this solute transport behavior. The DA model also assumes that the water and solute transport occurs by uncoupled diffusion across the membrane.

Figure 1 shows a cross section of a RO membrane with solute flux  $J_s$  through the membrane. By taking a

material balance around the slice  $\Delta z$  of the membrane and assuming  $J_s$  can be described by Fick's law, one can easily obtain

$$\frac{\partial C_m}{\partial t} = D_{sm} \frac{\partial^2 C_m}{\partial z^2} - \frac{\partial Q_m}{\partial t} \quad (10)$$

Equation 10 along with an expression for the rate of adsorption (adsorption rate =  $\partial Q_m/\partial t$ ) describes the concentration of solute in the membrane. Before the membrane feed is introduced, there is no solute in the membrane and so the initial condition is given by

$$C_m(0, z) = 0 \quad (11)$$

The boundary conditions are the same as those used in the MSD model:

$$C_{smf} = C_m(t, 0) = \frac{C_{tm} b_0 C_F}{1 + b_0 C_F} \quad (12)$$

$$C_{smp} = C_m(t, \delta) = \frac{C_{tm} b_0 C_P}{1 + b_0 C_P} \quad (13)$$

For dilute solutions, the permeate concentration can be eliminated from eq 13 using

$$C_P = \frac{J_s}{J_w} \quad (14)$$

along with the evaluation of  $J_s$  (by Fick's Law) at  $z = \delta$ .

Equations 10–12 and the modified  $C_m(t, \delta)$  equation can be rewritten in a more convenient form using the transformation  $x = z/\delta$  and  $D_e = D_{sm}/\delta^2$ . These equations then become

$$\frac{\partial C_m}{\partial t} = D_e \frac{\partial^2 C_m}{\partial x^2} - \frac{\partial Q_m}{\partial t} \quad (15)$$

$$C_m(0, x) = 0 \quad (16)$$

$$C_m(t, 0) = \frac{C_{tm} b_0 C_F}{1 + b_0 C_F} \quad (17)$$

$$C_m(t, 1) = \frac{-C_{tm} b_0 D_e \delta \frac{\partial C_m}{\partial x} \Big|_{x=1}}{J_w - b_0 D_e \delta \frac{\partial C_m}{\partial x} \Big|_{x=1}} \quad (18)$$

More importantly, once a profile has been obtained (using eqs 15–18), the permeate concentration can be found by rearranging eq 13 (with modifications) as

$$C_P = \frac{C_m(t, 1)}{b_0 [C_{tm} - C_m(t, 1)]} \quad (19)$$

It can be easily shown that the steady-state solution for the DA model is equivalent to the MSD model, as would be expected.

If equilibrium between the adsorbed and nonadsorbed diffusing solute is assumed to exist within the membrane, several adsorption isotherms can be used to describe the solute adsorption in the membrane. If

## D

Henry's law is assumed valid,

$$Q_m = Q_0 C_m \Rightarrow \frac{\partial Q_m}{\partial t} = Q_0 \frac{\partial C_m}{\partial t} \quad (20)$$

The DA model then becomes the DA–HA model,

$$\frac{\partial C_m}{\partial t} = \frac{D_e}{1 + Q_0} \frac{\partial^2 C_m}{\partial x^2} \quad (21)$$

If a Langmuir adsorption isotherm is assumed,

$$Q_m = \frac{Q_1 b_1 C_m}{1 + b_1 C_m} \Rightarrow \frac{\partial Q_m}{\partial t} = \frac{Q_1 b_1}{(1 + b_1 C_m)^2} \frac{\partial C_m}{\partial t} \quad (22)$$

and so the DA model becomes the DA–LA model,

$$\left[ 1 + \left( \frac{Q_1 b_1}{(1 + b_1 C_m)^2} \right) \right] \frac{\partial C_m}{\partial t} = D_e \frac{\partial^2 C_m}{\partial x^2} \quad (23)$$

All of the above equations can be solved with the appropriate boundary conditions, as discussed before. It should be noted that the DA model is not a pore model, but rather an extension of the MSD model to account for unsteady-state behavior. It can be easily shown that the steady-state solution of the DA model is equivalent to that of the MSD model.

For the incorporation of the transport model equations in a batch membrane system, the volume and concentration changes as a function of time must be included. For a batch system, a solute material balance results in

$$\frac{d(C_c V_c)}{dt} = 0 - A_m J_w C_p - \frac{dQ_{tm}}{dt} \quad (24)$$

where  $Q_{tm}$  represents the total solute adsorption in the membrane. Equation 24 can be expanded to

$$V_c \frac{dC_c}{dt} + C_c \frac{dV_c}{dt} = - A_m J_w C_p - \frac{dQ_{tm}}{dt} \quad (25)$$

From a material balance on the water with

$$r = \frac{V_p}{V_f} \quad (26)$$

then

$$V_c = V_f(1 - r) \Rightarrow \frac{dV_c}{dt} = - V_f \frac{dr}{dt} \quad (27)$$

Also,

$$\frac{dr}{dt} = \frac{A_m J_w}{V_f} \quad (28)$$

Combining eqs 27 and 28,

$$\frac{dV_c}{dt} = - A_m J_w \quad (29)$$

Substituting eqs 29 and 26 into eq 25 and rearranging results in

$$\frac{dC_c}{dt} = \frac{A_m J_w C_c - A_m J_w C_p - \frac{dQ_{tm}}{dt}}{V_f(1 - r)} \quad (30)$$

The system of eqs 28 and 30 along with expressions for the adsorption in the membrane, water flux ( $J_w$ ), and either solute flux ( $J_s$ ) or permeate concentration ( $C_p$ ) describe the batch membrane system. The initial conditions (at  $t = 0$ ) are  $r = 0$ ,  $C_c = C_F$ , and  $Q_{tm} = 0$ . The value of  $C_p$  obtained from the RO transport models is the instantaneous permeate concentration at time  $t$ . The cumulative permeate concentration for a batch system is defined as the concentration of the total volume of permeate collected up to a particular time or at a particular water recovery. It is calculated as

$$C_{pc} = \frac{\int_0^{V_p} C_p dV_p}{\int_0^{V_p} dV_p} \approx \frac{\sum_{i=1}^N C_p \Delta V_p}{\sum_{i=1}^N \Delta V_p} \quad (31)$$

**(3) Solution Techniques.** The solution of the MSD and the DA models requires the determination of the constants of the models as well as the implementation of a numerical solution routine. The parameters for the MSD model include  $A^*$ ,  $b_0$ , and  $B^*$ . The value of  $A^*$  was calculated using the distilled water flux of the membrane studied and eq 5:

$$A^* = \frac{J_{wo}}{\Delta P} \quad (32)$$

The parameters  $b_0$  and  $B^*$  were determined using a single experimentally determined data point for water flux and permeate and retentate concentration for all the solutes studied. The experimental point used was at 180 min for the batch membrane system. Although we used an experimental data point for the exact determination of  $b_0$ , it will be shown later how  $b_0$  can be estimated using solute acidity parameters. The value of  $b_0$  was determined using the experimental water flux and concentrate concentration using eq 5 (with  $C_F = C_c$ ) while  $B^*$  was determined using the measured permeate and concentrate concentrations and water flux with eqs 9 and 14. It should be noted that if we attempted to determine  $b_0$  from direct sorption experiments, the backing material sorption would mask the active layer sorption.

The parameters for the DA model include  $D_{sm}$ ,  $b_0$ ,  $C_{tm}$ , and  $\delta$  and the adsorption isotherm parameters  $Q_0$ ,  $Q_1$ , and  $b_1$ . To determine  $D_{sm}$  for the DA–HA and DA–LA models, it was assumed that diffusion of the solute in the membrane takes place through water dissolved in the membrane polymer. This water was assumed to be in the spaces (equivalent to pores) between the polymer chains of the membrane. Since the effective diffusivity of organic solutes through the membrane is unknown, the following equation was used to calculate the value of  $D_{sm}$ :

$$D_{sm} = \frac{D_{sw}}{b} \quad (33)$$

In eq 33, “*b*” is Ferry–Faxen-type friction parameter. On the basis of a large number of experimental membrane data, Sourirajan and Matsuura<sup>16</sup> have proposed that

$$b = 44.57 - 416.2\lambda + 934.9\lambda^2 + 302.4\lambda^3 \quad (34)$$

where  $\lambda = R_s/R_p$ . Equation 34 is valid for  $0.22 < \lambda < 1$ , which was true for all the solutes in this study. The diffusivities ( $D_{sw}$ ) for the solutes in water were calculated using the Wilke–Chang estimation method and Stoke’s radius ( $R_s$ ) for each solute. An average membrane “pore” radius ( $R_p$ ) was taken as 1 nm for the FT30 membrane used in this study.<sup>34</sup> The value of  $b_0$  was the same as that in the MSD model. For the DA–HA and DA–LA models the value of  $C_{tm}$  was determined using the steady-state solution of the DA model and single experimentally-determined values for the water flux and permeate and retentate concentrations at 180 min for the batch membrane system studied. The thickness of the membrane barrier layer was taken as 100 nm; this is in the range of values reported in the literature and that indicated by X-ray photoelectron spectroscopy (XPS) analysis as shown later.

The sets of equations describing a batch membrane system with the MSD and DA models were solved numerically to predict the permeate and retentate concentrations and water flux behavior. The MSD model was solved using the software package LSODE.<sup>35</sup> The DA model equations describing transport for a batch membrane system were solved using the NAG Fortran Library routine D03PJF. The routine uses a Chebyshev collocation method for the spatial discretization of the PDEs (partial differential equations) and either a backward differentiation formula (BDF) method or a Theta method for the integration of the resulting system of ODEs (ordinary differential equations).<sup>36</sup>

## Experimental Methods

**(1) Reverse Osmosis.** To quantify the permeation model parameters that were formulated and to establish organic separation behavior, experiments were conducted with thin-film, composite membranes in batch and continuous systems with various organic compounds. Preliminary characterization of the membrane by XPS was also done. The membrane feed, permeate, and retentate were analyzed by UV, high-performance liquid chromatography (HPLC), and a Hewlett-Packard 5890 gas chromatography-mass spectrometer (GC-MS). In some cases permeate concentrations were very low and then solid-phase extraction (described below) was used to concentrate the sample in a solvent phase.

The membranes used in all experiments was the FT30-BW membrane obtained in flat-sheet form from FilmTec Corp. It is a thin-film, composite membrane with a barrier layer of a cross-linked aromatic polyamide and support layer of porous polysulfone on a polyester backing. This membrane has a typical pure water flux of  $12 \times 10^{-4} \text{ cm}^3/(\text{cm}^2 \text{ s})$  and typical NaCl rejection of 97% at 1.4 MPa and 25 °C. The pH operating range is 2–11 with experiments being operated between 0% and 60% recovery.

The synthetic feed solutions used in the experiments were made by dissolving the appropriate chemicals in particle-free, double-distilled water. The organics used were phenol, 2-aminophenol (AP), 2-fluorophenol (FP), 2-chlorophenol (CP), 2,4-dichlorophenol (DCP), 2,4,6-

trichlorophenol (TCP), 2-nitrophenol (NP), 2,4-dinitrophenol (DNP), and benzene. The concentration and pH values were 0.1–0.5 mM and pH 3–5, respectively. Distilled water fluxes were measured before and after each membrane experiment to monitor the changes in membrane performances. If the water flux after the experiment was less than 80% of that before the experiment, the membrane was washed with a 20% methanol–water solution (or pH 9 water for ionizable organics) to remove adsorbed organics and restore the water flux. Performance was also periodically monitored using standard NaCl rejection for RO to ensure membrane stability and integrity.

Analysis was performed on HPLC or UV when possible, but when concentrations were low, GC-MS was used to accurately analyze the results. Of course, with all GC-MS analyses solid-phase extraction is needed since aqueous samples cannot be analyzed. The extraction was performed by filtering the aqueous samples (pH  $\approx$  4) through Fisher Scientific PrepSep C<sub>18</sub> (octadecyl silane) extraction columns, resulting in the retention of organics in the column. The adsorbed organic was then extracted from the column with methanol. Extraction efficiencies for CP, DCP, and TCP were nearly 100%.

Experimentation was done with two systems, a batch and continuous system. The batch system was used for the runs with recoveries ranging from 30% to 60%. The continuous system contained a large reservoir feed volume (85 L) with continuous recycling of the feed and permeate so that analysis could be ran with very little recovery ( $r \approx 0$ ). For the batch system, the membranes (in flat-sheet form) were placed in a 2.0-L stainless steel cylindrical pressure vessel (membrane surface area of 55 cm<sup>2</sup>) which was pressured with a nitrogen cylinder.<sup>37</sup> The solution in the cell served as the feed to the membrane and a variable speed mixer was ran at a rate of 900–1000 rpm to eliminate concentration polarization.

UV analyses of the various organic compounds were conducted at wavelengths ranging from 262 nm (DNP) to 292 nm (TCP) and had lower level detection limits of <0.01 mM (2 mg/L TCP). When GC-MS analysis was used, a solid-state extraction into methanol was used which gave an error of <3% (for example, 25 mg/L TCP read 25.8 mg/L) for all compounds used. For example, the amount of CP adsorbed by the membrane was 9.7% of the original amount in the feed solution. Using the error in the analysis ( $\pm 2 \text{ mg/L}$  chemical analysis), the mass balance was within 3% for model compounds known not to adsorb.

The elemental composition (on a hydrogen-free basis) of a FT30-BW membrane adsorbed with TCP were examined by XPS analysis. XPS was performed on a Kratos XSAM 800 spectrometer using Mg K $\alpha$ 1 (1253.6 eV) radiation. In situ argon ion sputtering was used to etch away the membrane barrier layer so that compositions as a function of depth could be obtained; the ion gun was operated at 3.5 keV with currents of 3- $\mu$ A across a sample area of around  $5 \times 25 \text{ mm}^2$ . The membrane was prepared by adsorbing TCP on it during a RO experiment with  $C_F = 0.25 \text{ mM}$ ,  $\text{pH}_F = 4$ , and 1.4 MPa. It was removed from the membrane system after the experiment and dried.

**(2) Nanofiltration.** The nanofiltration (NF) membrane used was the Desal HL membrane obtained in flat-sheet form from the Osmonics-Desal Corp. It is a negatively-charged, polyamide-based membrane on a

F

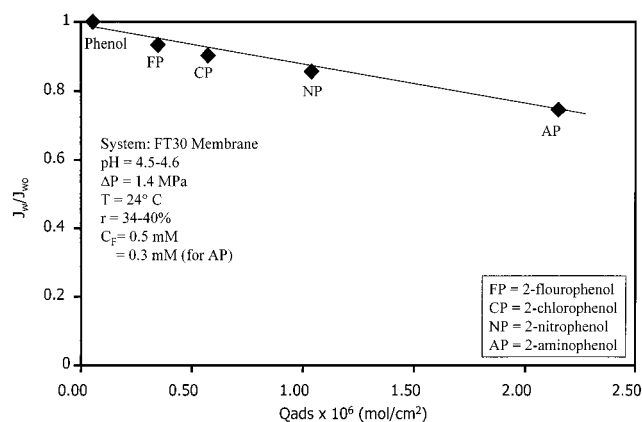


**Figure 2.** Relationship of water flux and organic adsorption for phenol and monosubstituted phenols.

polysulfone backing with a typical pure water flux of  $15 \times 10^{-4} \text{ cm}^3/(\text{cm}^2 \text{ s})$  and a typical 2000 mg/L  $\text{Na}_2\text{SO}_4$  rejection of 98% at 0.7 MPa and 25 °C. NF experiments with *p*-aminobenzoic acid (PABA) at a concentration of 100 mg/L and pH 3–9 consisted of using the batch system (described above for RO) with measurement of the flux, permeate, and retentate concentrations. Each flux reading was taken twice and experimentally measured fluxes agreed within 5%. Permeate and retentate concentrations were measured using a UV analysis (HP 8452A spectrophotometer) at 264 nm. Samples were diluted (if needed) to the concentration of 2–10 mg/L. The maximum and average standard errors of any analysis (done by determination of an unknown) was found to be 4% and 2%, respectively. Further, end retentate and permeate concentrations were measured and the mass balance was found to agree to within <2%.

## Results and Discussion

Extensive membrane studies were conducted to examine RO separation characteristics of dilute solutions of several hazardous organic pollutants. The behavior of most interest was water flux drop, organic removal, and extent of organic adsorption by the membrane and how these were related. Also, the RO models based on fundamental transport principles were solved and compared to the measured separation results to give insight into the transport mechanisms of organics in RO membranes. The usefulness of the models for describing water fluxes for organic systems were also examined. Finally, X-ray photoelectron spectroscopy (XPS) was analyzed to determine TCP adsorption in the membrane.

**(1) Organic Solute–Membrane Interactions.** Adsorption of organic membranes (FT30-BW) is thought to be a major factor contributing to flux drop. However, although many models are able to account for flux drop by manipulating empirical parameters, few look at how specific mechanisms of adsorption affect flux. Figure 2 shows flux drop versus adsorption for various monosubstituted phenols. As shown, the water flux decreases nearly linearly with adsorption. In addition to hydrogen-bonding effects, aminophenol (AP) caused the highest flux drop because of R– $\text{NH}_3$  interaction with a slightly negative FT30-BW membrane. An order of magnitude estimate of the potential organic loss (adsorption) was calculated for phenolic OH interaction with carbonyl groups. If the polymer is assumed to be homogeneous with a density of  $1 \text{ g/cm}^3$ , a polyamide barrier layer

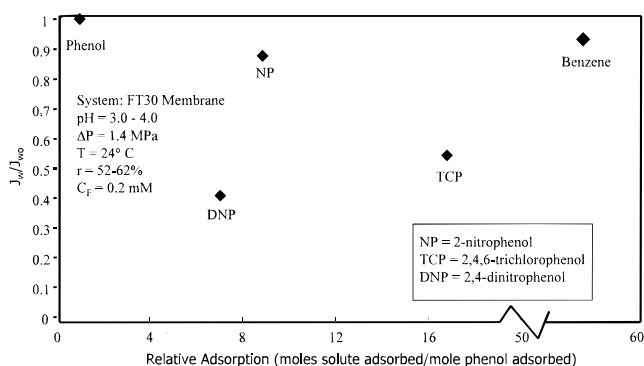


**Figure 3.** Water flux drop behavior with selected aromatics to distinguish the effect of specific (DNP and TCP) and nonspecific (benzene) adsorption.

thickness of 100 nm, and a membrane surface area of  $55 \text{ cm}^2$ , the maximum number of carbonyl groups available in the polymer would be  $5 \times 10^{-6} \text{ mol}$ . This is far less than the  $5 \times 10^{-5} \text{ mol}$  of TCP adsorbed at 0.24 mM, which indicates that some of the organics must also be adsorbed by nonspecific interactions.

For this reason, a TCP adsorption experiment was done with just the polysulfone backing (no active layer). Considering the fact that the concentration seen by the backing is only  $1/10$  of the 0.24 mM feed solute concentration (90% rejection), an adsorption of  $3 \times 10^{-7} \text{ mol/cm}^2$  was observed in the backing. This is approximately  $1/3$  of the overall adsorption, showing that the active layer indeed adsorbs a significant amount of the organics. Our scanning electron microscopy studies also indicated that the backing polysulfone layer has pore sizes in the range of 70–100 nm and thus adsorption of small molecules such as TCP on the pore surface will have no impact on the water flux. It should also be noted that Forgach et al.,<sup>45</sup> in their studies with FT-30 membranes, showed that transport parameters were characteristic of the polyamide barrier layer and the backing had no influence on flux or separation characteristics.

The degree of specific-to-nonspecific interactions can be very important, as indicated in Figure 3. As shown, DNP caused a very high water flux drop, even though NP had similar adsorption. This is because the disubstitution of the DNP highly enhances the molecule acidity. Figure 4 shows the possible hydrogen-bonding sites (using TCP as an example) with the FT30-BW membrane polymer. The carbonyl groups are the most likely interaction sites since the resonance structures of the amine–aromatic groups<sup>38</sup> of the aromatic polyamide would probably inhibit its formation of hydrogen bonds. In contrast, benzene with no hydrogen-bonding capability shows (Figure 3) high physical adsorption but negligible flux drop, showing that the reduction of transport corridors is not a phenomena leading to flux reduction.

Water flux through a RO membrane is thought to be greatly dependent on its ability to form hydrogen bonds with the hydrophilic groups of the membrane polymer; thus, water should be preferentially sorbed by the membrane polymer for the membrane to have high water fluxes.<sup>16</sup> Further, organics that form stronger hydrogen bonds with the membrane polymer than water would partially displace the water from the hydrophilic sites of the membrane. Therefore, a measure of hydrogen-bonding ability, such as the  $\text{p}K_a$ , should be a good indicator of water flux decline. Figure 5 indeed shows

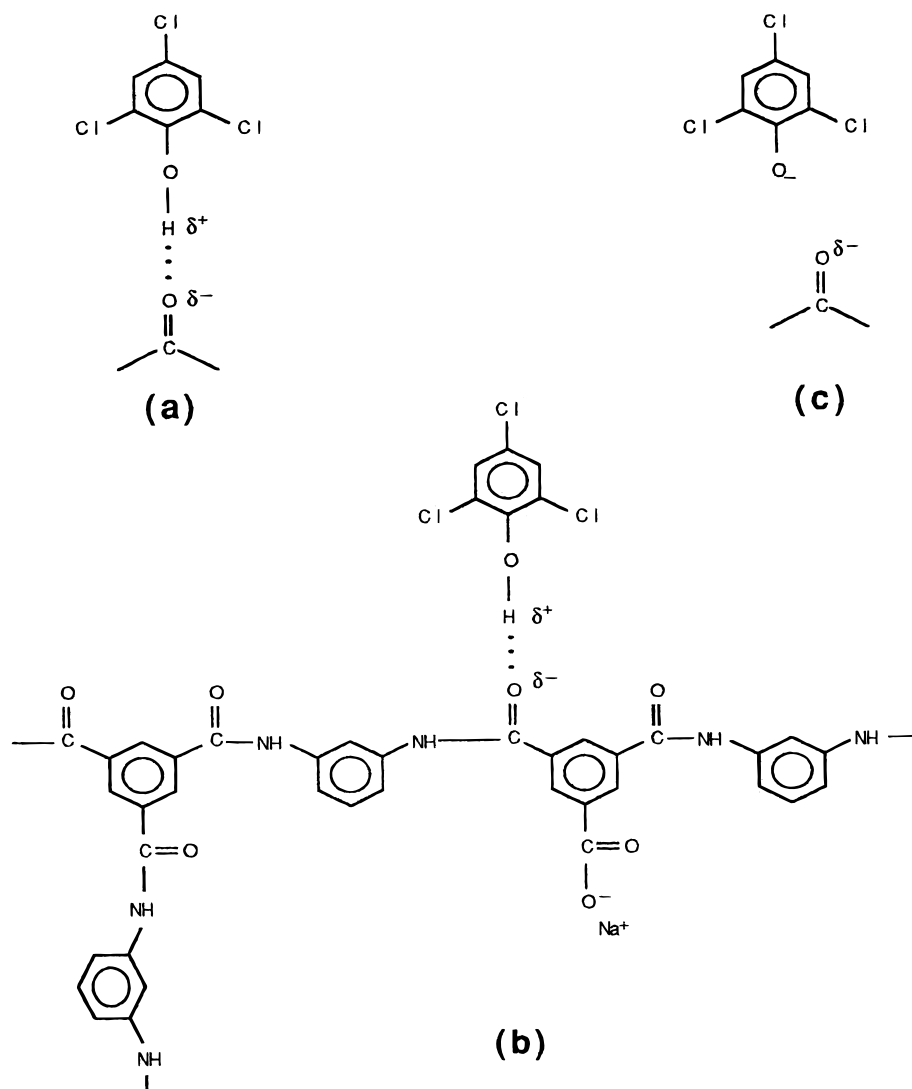


**Figure 4.** Schematic of interaction of nonionized trichlorophenol (TCP) with (a) carbonyl groups, (b) an aromatic polyamide RO membrane, and (c) ionized TCP with carbonyl groups.

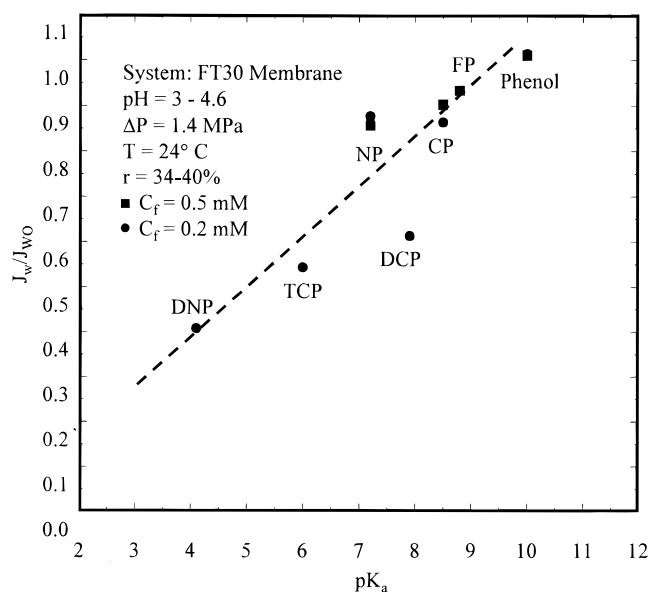


**Figure 5.** Water flux as a function of  $\text{p}K_a$  for selected phenolic compounds.

that the  $\text{p}K_a$  for the phenolics studied is a good measure of water flux decline. However, nonspecific interactions,

which may have little impact on flux, can be very important in terms of organic solute loss. For example, benzene, which is highly adsorbed in the membrane, causes no flux drop (Figure 3) but material loss (Figure 6) is very high. In contrast, phenol is a relatively polar compound which should have insignificant adsorption on the membrane (Figure 3). For the chlorophenols, each addition of chlorine would make the compound more hydrophobic and thus cause an increase in physical adsorption by the membrane. The concepts of specific and nonspecific interactions are consistent with the behavior observed for some of the phenolics under ionized conditions. When ionized, these compounds cause substantially less water flux drop with the FT30-BW membranes.<sup>3</sup> The water flux through composite RO membranes (e.g., FT30-BW) obviously is a function of the skin thickness. Although the absolute value of the flux (and organic adsorption) will increase with membrane skin thickness, the percentage flux drop will remain the same.

Evidence of the importance of specific interactions can further be verified by the analysis of transient flux and permeate concentration behavior. Figure 7 shows the flux and permeate concentration variation with time involving insignificant water recovery (both permeate

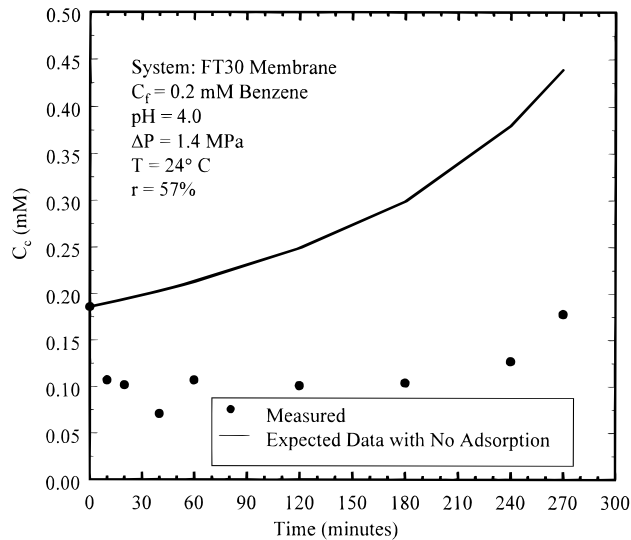


**Figure 6.** Effect of benzene adsorption on retentate concentration variation with time.

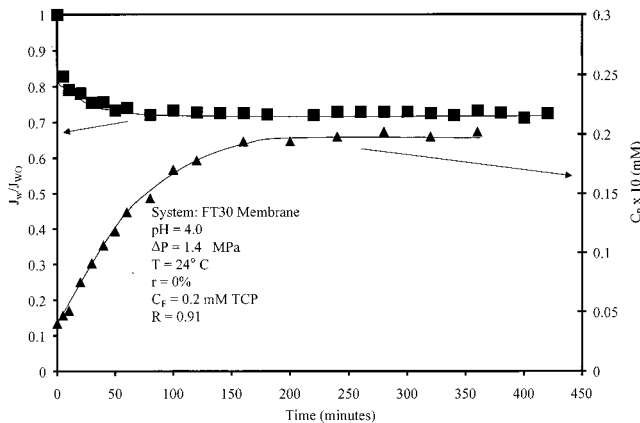


**Figure 7.** Water flux drop and permeate concentration behavior of TCP for a RO experiment with negligible water recovery.

and retentate recycled back to the feed tank). If, overall, nonspecific adsorption controlled the water flux, then one would expect, on one hand, a continual flux drop over a long period of time. On the other hand, permeate concentration would be expected to increase with time until steady state is reached. The rapid attainment of steady-state flux (Figure 7) does indicate the importance of specific interactions with water transport sites in the membranes. The total concentration  $C_{tm}$  (eq 2) can be viewed as representing the total number of membrane interaction sites that can be occupied by the organic solute and water. Although water is present in considerable excess, competitive sorption was evident by the experimental  $b_0$  (eq 4) values dependency on feed solute concentration. For example, with TCP in the concentration range of 0.1–0.5 mM, the quantity  $b_0 C_F$  was approximately linear with the feed concentration. With organics that have strong interactions with the membrane (that is, a large  $C_m$  due to either hydrogen bonding or hydrophobic forces), the concentration of water in the membrane would decrease, thus causing flux decline. This is in agreement with the findings of Burghoff et al.<sup>18</sup> and Rautenbach and Gröschl<sup>31–33</sup> who found that some organics could decrease the membrane water content. Cheng et al.,<sup>14</sup> in their detailed studies with various halogenated organics, found that the membrane void fraction (measure of water content)

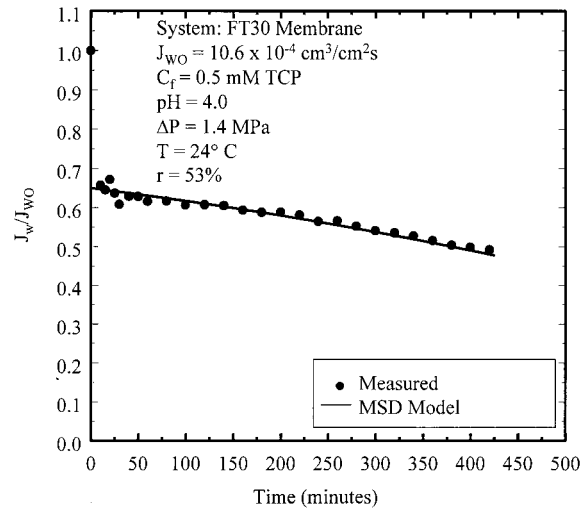


**Figure 8.** Measured and calculated (MSD model) water flux as a function of time for a batch RO experiment.

indeed decreased (20%–50%), depending on the membrane and organic solute utilized.

**(2) MSD Model Verification.** The MSD model has been used for the prediction of permeate concentration and water flux behavior. While the equations describe the unsteady-state nature of the batch system, these assume the membrane itself has steady-state partitioning and diffusion of organics and water. Water flux results for the MSD model for a 0.5 mM TCP feed solution ( $b_0 = 1380$  L/mol,  $A^* = 7.70 \times 10^{-4}$  cm/(s MPa), and  $B^* = 0.569 \times 10^{-10}$  mol/(cm<sup>2</sup> s)) are given in Figure 8. Since the feed was continuously concentrated with operating time, the batch membrane system represented a convenient test of the model over a range of concentrations. This verified that the continuous drop in water flux for the batch system was the result of increases in retentate concentration over time and that eq 5 could adequately describe the changes in water flux due to the feed solute concentration changes. In addition, the retentate concentration variation indicated (not shown here) that fit between the MSD model and experimental data was within 8%.

The cumulative permeate concentrations variation with time was also modeled, and as expected, the steady-state behavior can be predicted quite well, as indicated in Figure 9 (using the same membrane parameters as Figure 8). The steady-state results showed about 90% rejection of TCP for this membrane.<sup>3</sup> However, the MSD model overpredicted the permeate concentration, especially for the lower operating times. This disagreement was most likely due to unsteady-state solute transport in the membrane just after the experiments were started. The unsteady-state behavior would not be described by the MSD model since it assumed steady-state conditions in the membrane. Thus, it is clear that other models are needed to describe the unsteady-state behavior of permeate concentration data.

Parametric studies for membrane models are important since these allow insight into the effect a particular variable or constant might have on water flux or separation characteristics. Further, parametric studies can point out some potential improvements that can be made for a membrane to optimize water fluxes or separations. Using the information of the MSD model, various predictions of membrane behavior can be made.

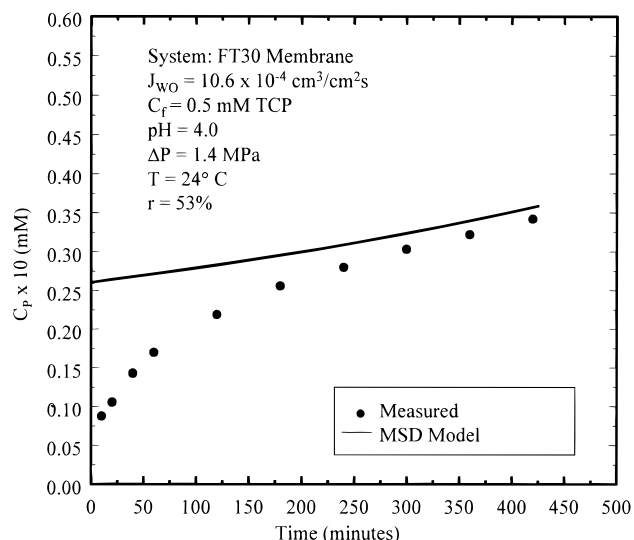


**Figure 9.** Calculated (MSD model) and experimental permeate TCP concentration for a batch RO experiment.

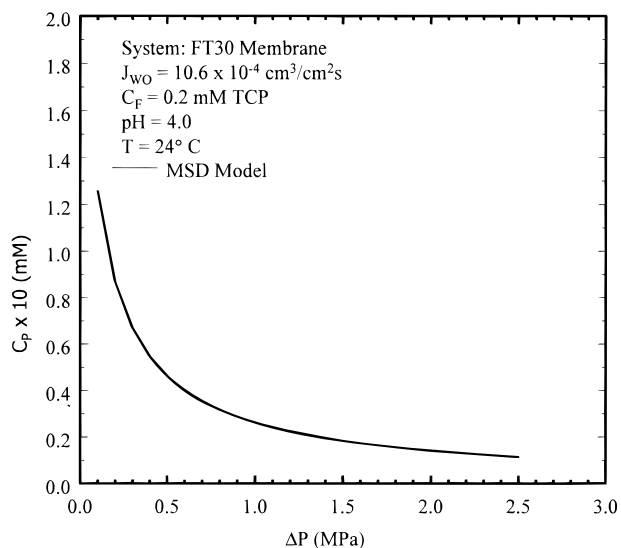


**Figure 10.** Modified solution diffusion model (MSD) predicted permeate concentration as a function of operating pressure for dilute aqueous TCP.

The model must predict the trend that permeate concentrations should reach an asymptotic number as the pressure is increased. As can be seen in Figure 10, this is indeed the case.

The specific sorption coefficient parameter,  $b_0$  (in eq 5), which is a measure of specific interactions, should have a strong impact on the water flux drop behavior. This effect in Figure 11 shows that in the dilute concentration range (negligible osmotic pressure) the flux drop is quite severe for high values of  $b_0$ . Figure 11 also indicates that higher solute feed concentrations would result in larger water flux drops, which would be expected on the basis of eq 5. From our experimental observations, it has already been noted that strongly acidic compounds, such as DNP, cause severe membrane flux decline and thus one would expect that  $b_0$  would be a strong function of acidity. Figure 12 shows the strong dependence of solute acidity ( $pK_a$ ) on the best fit  $b_0$  parameters (at 0.2 mM) for various phenolic compounds. Further understanding of the importance of organic sorption on membranes will not only help one to describe flux drop behavior (without membrane

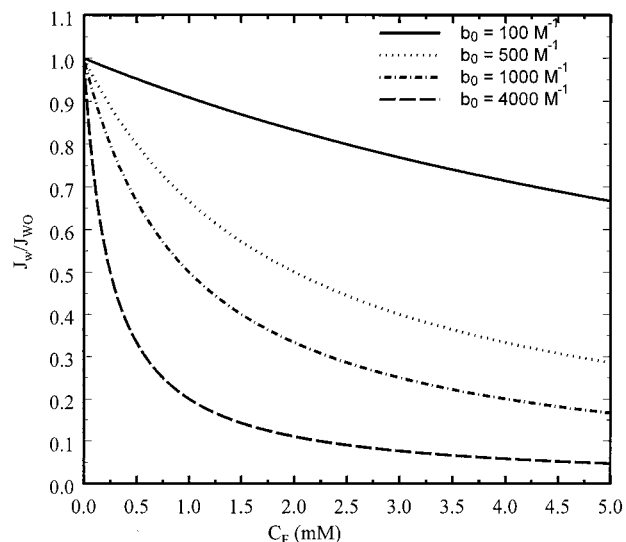


**Figure 11.** Effect of the sorption coefficient parameter,  $b_0$ , on water flux calculated by the MSD model as a function of feed concentration.

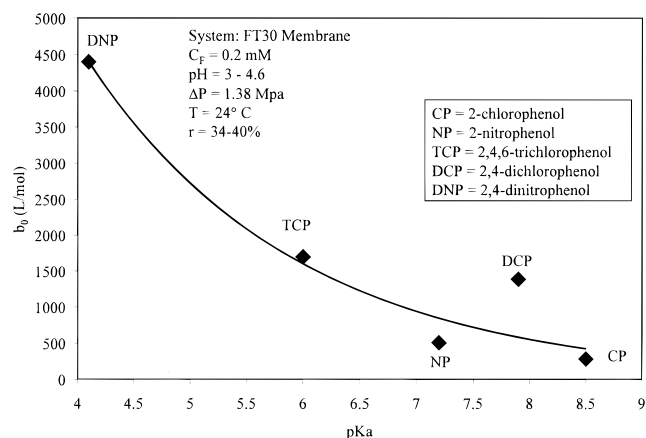


**Figure 12.** Correlation of the MSD model sorption coefficient parameter,  $b_0$ , with  $pK_a$  of selected phenolic compounds.

experimentation) but also may lead to the development of “adsorptive membranes”.

**(3) Diffusion–Adsorption (DA) Models.** A likely cause for the unsteady-state behavior of the dilute organic solute flux is that the solute adsorbs in the membrane as it is transported through it. Equations 21 and 23 (DA–HA and DA–LA models, respectively) along with the boundary conditions and the batch equations describe unsteady-state diffusion with Henry’s-law or Langmuir-type adsorption in the membrane. The isotherms utilized are widely applied to organic adsorption and have been indicated to describe membrane adsorption: a linear adsorption isotherm.<sup>39</sup> Equation 21 is particularly enlightening. Crank<sup>40</sup> pointed out that this is the usual one-dimensional form of the diffusion equation with the exception that the diffusion coefficient is reduced by the factor  $(1 + Q_0)$ . Numerical solutions of eq 21 (DA–HA model) and related equations for the batch system permeate concentration for the 0.5 mM TCP feed solution with several values of Henry’s law coefficient  $Q_0$  are shown in Figure 13. The parameters used for the DA model are  $b_0 = 1380$  L/mol,  $R_s = 0.31$  nm,  $D_{sw} = 7.68 \times 10^{-6}$  cm<sup>2</sup>/s,  $D_{sm} = 5.26 \times 10^{-7}$  cm<sup>2</sup>/s, and  $C_{tm} = 1.08 \times 10^{-6}$  mol/L. The figure shows that as  $Q_0$  increases (and so adsorption increases), the overall effective rate of diffusion  $[D_e/(1 + Q_0)]$  decreases. Thus,

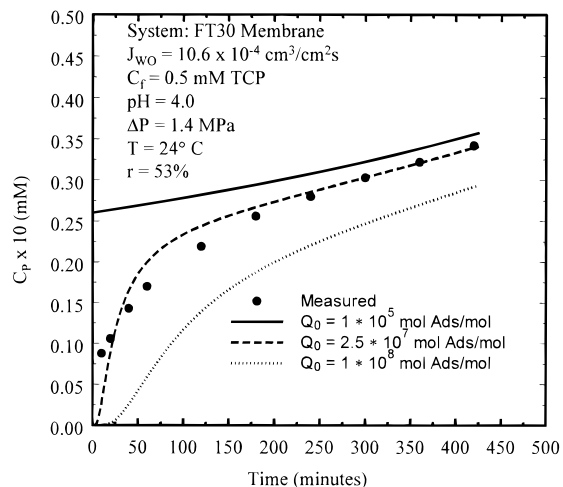


**Figure 13.** Comparison of experimental and diffusion–Henry's law adsorption (DA–HA) based permeate TCP concentration.

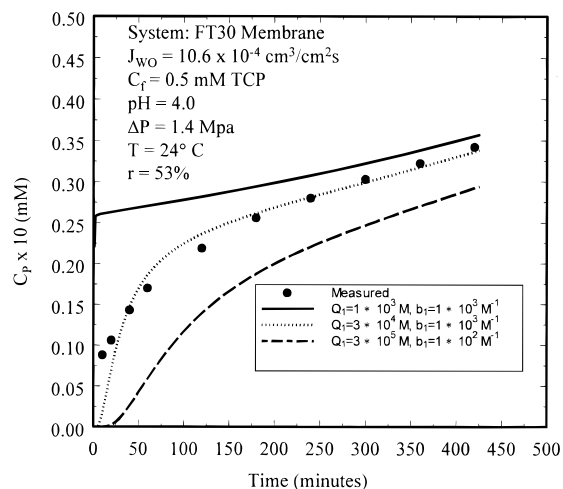


**Figure 14.** Calculated (diffusion–Langmuir adsorption based DA–LA model) and experimental permeate concentration profile for TCP.

one would expect a strong dependence of the  $Q_0$  parameter on the permeate concentration time profile. More importantly, this plot shows that the effect of adsorption is to lower the overall solute diffusivity. For a TCP diffusivity of  $D_{sm} = 5.26 \times 10^{-7} \text{ cm}^2/\text{s}$  in the membrane and  $Q_0 = 2.5 \times 10^7 \text{ mol adsorbed/mol}$ ,  $D_{sm}/(1 + Q_0) \approx 2 \times 10^{-14} \text{ cm}^2/\text{s}$ . This is on the order of the TCP membrane diffusivities found.

Figure 14 shows numerical solutions for eq 23 (DA–LA model) and related batch membrane equations where the adsorption is described by a Langmuir isotherm with several values of the adsorption coefficients  $Q_1$  and  $b_1$  for a 0.5 mM TCP feed solution. The cumulative permeate curves show trends similar to those in Figure 13. In fact, this would be expected since the TCP concentrations in the membrane should be low (90% rejection as well as low feed concentration) and, as a result, the Langmuir isotherm would reduce to a linear form (Henry's law); that is,  $Q_0 = Q_1 b_1$ . The fact that constant values of  $Q_1 b_1$  shown in the figure produced approximately the same numerical solution also indicates that the Langmuir isotherm reduced to a linear form for the concentrations present in the membrane.

**(4) XPS Characterization of the FT30-BW Membrane.** The FT30-BW membrane used in this study was

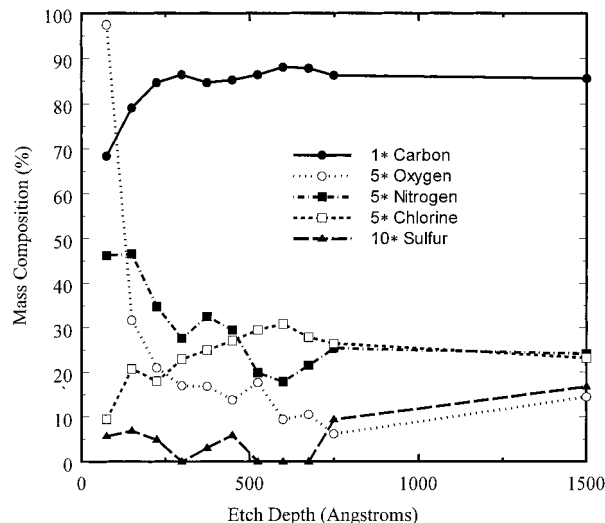
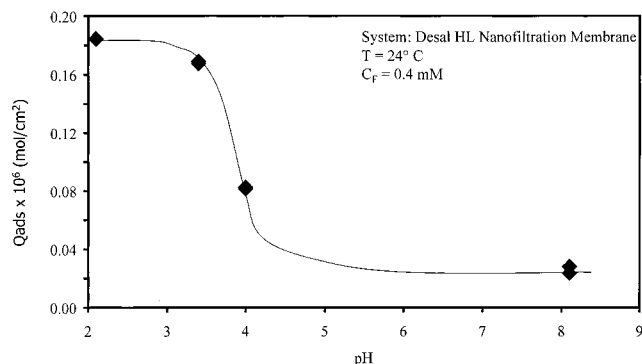


**Figure 15.** XPS (X-ray photoelectron spectroscopy) profile of elemental mass composition for a TCP adsorbed FT30-BW membrane.

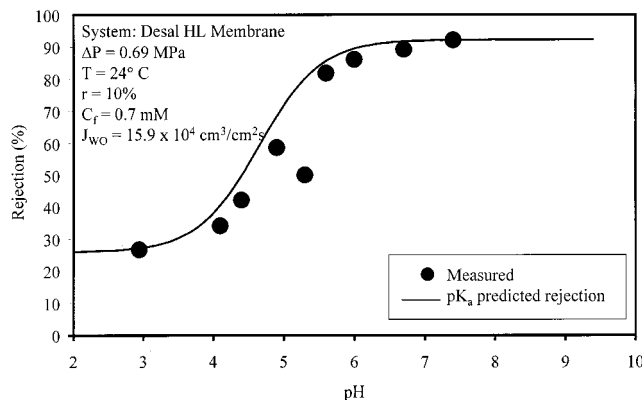
analyzed by XPS, which allows relatively precise determination of elemental compositions. A membrane with TCP adsorbed was examined and the composition (only Cl in the membrane came from TCP) was determined as a function of depth by etching the polymer with argon ion ( $\text{Ar}^+$ ) sputtering. The analysis of the membrane was performed to examine the distribution of the adsorbed TCP in the barrier layer. Under the sputtering conditions used, the etching rate of a  $\text{SiO}_2$  standard film has been estimated as 2.5 nm/min;<sup>41</sup> since it would be very difficult to determine the etching rate of the membrane polymer film due to the lack of a similar standard, the  $\text{SiO}_2$  etching rate can be used as a first approximation to that of the polymer.

Figure 15 shows the compositions of carbon, nitrogen, oxygen, sulfur, and chlorine in the membrane for several XPS scans for the membrane adsorbed with TCP. The TCP was adsorbed during a RO experiment with  $C_F = 0.2 \text{ mM}$  and  $1 \times 10^{-6} \text{ mol/cm}^2$  TCP was adsorbed by the membrane during the experiment. Since the barrier layer polyamide or the support layer polysulfone did not contain chlorine, the percentage of chlorine indicated in Figure 15 must be due to the TCP in the membrane. Since the aromatic polyamide barrier layer contained no sulfur, the sulfur composition should increase only when the polysulfone layer is reached. This is found to be at a depth between 75 and 150 nm (30–60 min of etching) as indicated in Figure 15.

**(5) Organic Adsorption and Rejection Behavior for NF Membranes.** Charged NF membranes are used for the separation of many organic molecules. A comprehensive view of all the MW cutoffs of NF membranes is given by Rautenbach and Mellis.<sup>42</sup> Since a significant amount of work had been performed on RO adsorption studies, NF membranes were characterized with a model organic compound to establish the role of adsorption and pH on membrane performance. The model compound chosen for the study was *p*-aminobenzoic acid (PABA). PABA is an interesting molecule from a research standpoint because it has a positive charge at low pH (amine  $\text{p}K_a = 4.65$ ) and a negative charge at higher pH's (carboxyl  $\text{p}K_a = 4.80$ ). Although PABA is a molecule similar to many of the compounds studied in this article, the adsorption on a NF membrane would be assumed to be lower because it is much more hydrophilic



**Figure 16.** Effect of pH on PABA (*p*-aminobenzoic acid) adsorption by negatively-charged NF membranes.



**Figure 17.** Effect of pH on PABA rejection with negatively charged NF membranes.

than FT-30 and many researchers have shown that this hydrophilicity leads to lower protein sorption, for instance.<sup>43</sup> In addition, one would expect organics containing positive charges, such as amine groups, to have stronger interactions with negatively-charged membranes.<sup>44</sup> Figure 16 shows that the adsorption of PABA on the Desal-HL membrane is as much as a factor of 10 lower than 2-aminophenol (AP) sorption on FT-30BW. However, it is also interesting to note that the adsorption of PABA on the membrane is a function of pH. This is probably due to charge interaction (negatively-charged membrane) of positive amine at low pH and charge repulsion of negatively-charged carboxyls at high pH. In FT-30BW membranes the mechanisms of water transport is primarily diffusion which is facilitated through interactions with specific sites on the membrane. However, the Desal-HL membrane is negatively-charged and transport through this membrane is probably a function of convection, diffusion, and electrical interactions (negatively-charged membrane facilitating water diffusion). In this work, we found that the Desal-HL membrane flux was about 5% lower than the pure water flux at all pH values, showing that the change in adsorption caused insignificant flux decline. This membrane is highly hydrophilic and thus one would not expect significant flux drop with low-molecular-weight organic solutes.

PABA has two charge groups and thus one would expect a strong impact of pH on the separation. The pH effect can be easily explained on the basis of ionization ( $pK_a$ ). Figure 17 is a plot of PABA rejection vs pH. It can be shown that even at pH 3 ( $\approx 100\%$  positively charged) PABA was rejected around 25%. Also shown in Figure 17, a model for the rejection based on ionization is also plotted. The model utilized only two data

points: one around pH 3 and one above pH 7. As shown, the model predicted NF rejection reasonably well.

## Conclusions

This study examined water flux, separation, and adsorption for several hazardous organic pollutants by a thin-film, composite membrane (FT30-BW). Models were developed on the basis of fundamental transport principles which included the effects of organic sorption/adsorption that were formulated and solved to describe water fluxes and separations for the organic systems studied. Studies with several nonionized, ortho-substituted phenolic compounds in dilute solutions (negligible osmotic pressure) showed that these could cause substantial decreases in water flux through the membrane. Material balances on the system also indicated significant organic adsorption by the membrane (on the order of  $10^{-6}$  mol/cm<sup>2</sup>) during the RO experiment. It was found that both water flux drop and adsorption followed the same trends for these phenolics: AP > NP > CP > FP > phenol. Selected nonionized chlorophenols and nitrophenols in dilute solutions (negligible osmotic pressure) were studied and also found to cause substantial membrane water flux drop for some cases. The order of flux drop for these for similar feed concentrations was DNP > TCP > DCP > CP > NP. Flux drop results were explained in terms of specific and nonspecific interactions. Studies with a continuous RO system showed that water flux drops caused by TCP occurred rapidly and reached a steady-state value. However, the permeate concentration clearly showed a transient behavior, increasing with operating time.

Reverse osmosis transport models were formulated to describe water flux and separations for organics systems. The modified solution-diffusion (MSD) model and diffusion-adsorption (DA) models were solved numerically for selected organics. The parameters of the models were obtained from measured data at a single data point. The MSD and DA models gave excellent descriptions of water flux (typically within 5%) for the phenolics studied. The MSD model did predict the steady-state behavior of the permeate concentration quite accurately, while DA models were needed for the successful prediction of transient concentration profiles. With charged NF membranes (loose RO), the flux drop was not found to be significant despite some organic adsorption. The separation behavior of a model compound containing two ionizable groups (one positive and one negative) could be predicted quite well with  $pK_a$  data.

## Nomenclature

- $A$  = water permeability coefficient, ( $L^3/L^2tP$ )
- $A^*$  = modified water permeability constant, ( $L^3/L^2tP$ )
- $A_m$  = membrane surface area,  $L^2$
- $b$  = solute-membrane friction parameter, dimensionless
- $B^*$  = modified solute permeability constant, ( $mol/L^2t$ )
- $b_0$  = sorption coefficient,  $L^3/mol$
- $b_1$  = Langmuir adsorption coefficient,  $L^3/mol$
- $C_c$  = concentrate solute concentration,  $mol/L^3$  or  $M/L^3$
- $C_f$  = feed solute concentration,  $mol/L^3$  or  $M/L^3$
- $C_m$  = membrane solute concentration,  $mol/L^3$
- $C_p$  = permeate solute concentration,  $mol/L^3$  or  $M/L^3$
- $C_{pc}$  = cumulative permeate solute concentration,  $mol/L^3$  or  $M/L^3$
- $C_{smf}$  = solute concentration at feed side membrane surface,  $mol/L^3$

## L

$C_{\text{sm}} =$  solute concentration at permeate side membrane surface, mol/L<sup>3</sup>  
 $C_{\text{tm}} =$  total concentration of water and solute in the membrane, mol/L<sup>3</sup>  
 $C_{\text{wm}} =$  membrane water concentration, mol/L<sup>3</sup>  
 $D_e =$  normalized solute diffusivity,  $D_{\text{sm}}/\delta^2$ , 1/t  
 $D_{\text{sm}} =$  solute diffusivity in membrane, L<sup>2</sup>/t  
 $D_{\text{sw}} =$  solute diffusivity in water, L<sup>2</sup>/t  
 $D_{\text{wm}} =$  water diffusivity in membrane, L<sup>2</sup>/t  
 $J_s =$  solute flux, mol/(L<sup>2</sup>t) or M/(L<sup>2</sup>t)  
 $J_w =$  water flux, L<sup>3</sup>/(L<sup>2</sup>t)  
 $J_{\text{wo}} =$  pure water flux, L<sup>3</sup>/(L<sup>2</sup>t)  
 $K_{\text{sm}} =$  solute partition coefficient for homogeneous membrane, dimensionless  
 $L =$  length  
 $L_{\text{sp}} =$  pressure-induced solute transport parameter, mol/(L<sup>2</sup>tP) or M/(L<sup>2</sup>tP)  
 $M =$  mass  
 $P =$  pressure, M/(L<sup>2</sup>)  
 $Q_m =$  solute adsorption in membrane, mol/L<sup>3</sup>  
 $Q_{\text{tm}} =$  total solute adsorption in membrane, mol  
 $Q_0 =$  Henry's law adsorption coefficient, mol adsorbed/mol  
 $Q_1 =$  Langmuir adsorption coefficient, mol/L<sup>3</sup>  
 $r =$  permeate water recovery, dimensionless  
 $R_g =$  ideal gas constant, (ML<sup>2</sup>)/(t<sup>2</sup>T mol)  
 $R_p =$  membrane pore radius, L  
 $R_s =$  Stoke's radius of solute, L  
 $t =$  time  
 $T =$  temperature  
 $V_c =$  concentrate volume, L<sup>3</sup>  
 $V_F =$  feed volume, L<sup>3</sup>  
 $V_P =$  permeate volume, L<sup>3</sup>  
 $\bar{V}_w =$  partial molar volume of water, L<sup>3</sup>/mol  
 $x =$  dimensionless membrane depth,  $z/\delta$   
 $z =$  membrane depth, L

### Greek Letters

$\delta =$  membrane thickness, L  
 $\lambda =$  ratio of solute Stoke's radius to membrane pore radius, dimensionless  
 $\Delta\pi =$  transmembrane osmotic pressure difference, M/(L<sup>2</sup>)

### Chemical Abbreviations

AP = 2-aminophenol  
CP = 2-chlorophenol  
DCP = 2,4-dichlorophenol  
DNP = 2,4-dinitrophenol  
FP = 2-fluorophenol  
NP = 2-nitrophenol  
PABA = *p*-aminobenzoic acid  
TCP = 2,4,6-trichlorophenol

### Acknowledgment

This work was supported in part by a grant from the National Science Foundation (CTS 9307518). J. Hestekin was supported by a NSF-IGERT fellowship. C. Smothers was a NSF-REU student. The NF membranes were supplied by the Osmonics-Desal Corporation. The authors also acknowledge NIST-ATP and SmithKline Beecham for partial support of this work.

### Literature Cited

(1) Ho, W., Sirkar, K., Eds. *Membrane Handbook*; Van Nostrand Reinhold: New York, 1992.  
(2) Soltanieh, M.; Gill, W. Review of Reverse Osmosis Membranes and Transport Models. *Chem. Eng. Commun.* **1981**, *12*, 279–363.  
(3) Bhattacharyya, D.; Mangum, W. C.; Williams, M. E. Reverse Osmosis. In *Encyclopedia of Environmental Analysis and Remediation*; John Wiley: New York, 1998; pp 4149–4165.

(4) Lonsdale, H.; Merten, U.; Riley, R. Transport Properties of Cellulose Acetate Osmotic Membranes. *J. Appl. Polym. Sci.* **1965**, *9*, 1341.  
(5) Sherwood, T.; Brian, P.; Fisher, R. Desalination by Reverse Osmosis. *Ind. Eng. Chem. Fundam.* **1967**, *6*, 2.  
(6) Matsuura, T.; Sourirajan, S. Physicochemical Criteria for Reverse Osmosis Separation of Alcohols, Phenols, and Monocarboxylic Acids in Aqueous Solutions Using Porous Cellulose Acetate Membranes. *J. Appl. Polym. Sci.* **1971**, *15*, 2905–2927.  
(7) Hestekin, J. A.; Bhattacharyya, D.; Sikdar, S. K.; Kim, B. M. Applications of Membranes for Treatment of Hazardous Wastewaters. In *Encyclopedia of Environmental Analysis and Remediation*; John Wiley: New York, 1998; pp 2685–2708.  
(8) Kastelan-Kunst, L.; Kosutic, K.; Dananic, V.; Kunst, B. FT30 Membranes of Characterized Porosities in the Reverse Osmosis Organics Removal From Aqueous Solutions. *Water Res.* **1997**, *31*, 2878–2884.  
(9) Reimann, W. Influence of Organic Matter from Waste Water on the Permeability of Membranes. *Desalination* **1997**, *109*, 51–55.  
(10) Rosa, M. J.; Norberta de Pinho, M. Separation of Organic Solutes by Membrane Pressure-Driven Processes. *J. Membr. Sci.* **1994**, *89*, 235–243.  
(11) Todtheide, V.; Laufenberg, G.; Kunz, B. Waste Water Treatment Using Reverse Osmosis: Real Osmotic Pressure and Chemical Functionality as Influencing Parameters on the Retention of Carboxylic Acids in Multi-Component Systems. *Desalination* **1997**, *110*, 213–222.  
(12) Laufenberg, G.; Hausmanns, S.; Kunz, B. The Influence of Intermolecular Interactions on the Selectivity of Several Organic Acids in Aqueous Multicomponent Systems During Reverse Osmosis. *J. Membr. Sci.* **1996**, *110*, 59–68.  
(13) Pusch, W.; Yu, Y. L.; Zheng, L. Y. Solute–Solute and Solute–Membrane Interactions in Hyperfiltration of Binary and Ternary Aqueous Organic Feed Solutions. *Desalination* **1989**, *75*, 3–14.  
(14) Cheng, R.; Glater, J.; Neethling, J. B.; Stenstrom, M. K. The Effects of Small Halocarbons on RO Membrane Performance. *Desalination* **1991**, *85*, 33–44.  
(15) Dickson, J. M.; Whitacker, G.; DeLeeuw, J.; Spencer, J. Dilute Single and Mixed Solute Systems in a Spiral Wound Reverse Osmosis Module Part II. Experimental Data and Application of the Model. *Desalination* **1994**, *99*, 1–18.  
(16) Sourirajan, S.; Matsuura, T. *Reverse Osmosis/Ultrafiltration Principles*; National Research Council of Canada: Ottawa, Canada, 1985.  
(17) Bhattacharyya, D.; Back, S.; Kermod, R. Prediction of Concentration Polarization and Flux Behavior in Reverse Osmosis by Numerical Analysis. *J. Membr. Sci.* **1990**, *48*, 231–262.  
(18) Burgoff, H. G.; Lee, K. L.; Pusch, W. Characterization of Transport Across Cellulose Acetate Membranes in the Presence of Strong Solute–Membrane Interactions. *J. Appl. Polym. Sci.* **1980**, *25*, 323–347.  
(19) Sourirajan, S. *Reverse Osmosis*; Academic Press: New York, 1970.  
(20) Kimura, S.; Sourirajan, S. Analysis of Data in Reverse Osmosis with Porous Cellulose Acetate Membranes Used. *AIChE J.* **1967**, *13*, 497–503.  
(21) Trushinski, B. J.; Dickson, J. M.; Smyth, T.; Childs, R. F.; McCarry, B. E. Polysulfonamide Thin-Film Composite Reverse Osmosis Membranes. *J. Membr. Sci.* **1998**, *143*, 181–188.  
(22) Dickson, J. M.; Spencer, J.; Costa, M. L. Dilute Single and Mixed Solute Systems in a Spiral Wound Reverse Osmosis Module Part I: Theoretical Model Development. *Desalination* **1992**, *89*, 63–88.  
(23) Merten, U. Transport Properties of Osmotic Membranes. In *Desalination by Reverse Osmosis*; Merten, U., Ed.; MIT Press: Cambridge, MA, 1966; pp 15–54.  
(24) Jonsson, G.; Boesen, C. Water and Solute Transport Through Cellulose Acetate Reverse Osmosis Membranes. *Desalination* **1975**, *17*, 145–165.  
(25) Mehdizadeh, H.; Dickson, J. M. Theoretical Modification of the Finely Porous Model for Reverse Osmosis Transport. *J. Appl. Polym. Sci.* **1991**, *42*, 1143–1154.  
(26) Niemi, H.; Palosaari, S. Flowsheet Simulation of Ultrafiltration and Reverse Osmosis Processes. *J. Membr. Sci.* **1994**, *91*, 111–124.

- (27) Mehdizadeh, H.; Dickson, J. M. Modeling of Reverse Osmosis in the Presence of Strong Solute-Membrane Affinity. *AIChE J.* **1993**, *39*, 434–445.
- (28) Hall, M. S.; Starov, V. M.; Lloyd, D. R. Reverse Osmosis of Multicomponent Electrolyte Solutions Part I. Theoretical Development. *J. Membr. Sci.* **1997**, *128*, 23–37.
- (29) Peeters, J. M. M.; Boom, J. P.; Mulder, M. H. V.; Strathmann, H. Retention Measurements of Nanofiltration Membranes with Electrolyte Solutions. *J. Membr. Sci.* **1998**, *145*, 199–209.
- (30) Bowen, W. R.; Mukhtar, H. Characterisation and Prediction of Separation Performance of Nanofiltration Membranes. *J. Membr. Sci.* **1996**, *112*, 263–274.
- (31) Rautenbach, R.; Gröschl, A. Reverse Osmosis of Aqueous–Organic Solutions: Material Transport and Process Design. Presented at the 1990 International Congress on Membranes and Membrane Processes, Chicago, IL, Aug 20–24, 1990.
- (32) Rautenbach, R.; Gröschl, A. Fractionation of Aqueous Organic Mixtures by Reverse Osmosis. Presented at the 203rd American Chemical Society National Meeting, San Francisco, CA, April 5–10, 1992.
- (33) Rautenbach, R.; Groschl, A. Fractionation of Aqueous Organic Mixtures by Reverse Osmosis. *Desalination* **1993**, *90*, 93–106.
- (34) Bhattacharyya, D.; Jevtitch, M.; Schrodt, J.; Fairweather, G. Prediction of Membrane Separation Characteristics by Pore Distribution Measurements and Surface Force-Pore Flow Model. *Chem. Eng. Commun.* **1986**, *42*, 111–128.
- (35) Hindmarsh, A. LSODE and LSODI, Two New Initial Value Ordinary Differential Equation Solvers. *ACM-SIGNUM Newsletter* **1980**, *15*, 10.
- (36) NAG. D03-Partial Differential Equations. In *The NAG Fortran Library Manual, Mark 15*; The Numerical Algorithms Group Limited: Oxford, United Kingdom, 1991.
- (37) Williams, M.; Deshmukh, R.; Bhattacharyya, D. Separation of Hazardous Organics by Reverse Osmosis Membranes. *Environ. Prog.* **1990**, *9*, 118–125.
- (38) Loudon, G. *Organic Chemistry*; Addison-Wesley: Reading, MA, 1984.
- (39) Murphy, A. Cellulose Acetate: Interactions with Aqueous Phenol and a Transition Temperature of about 20 C. *J. Appl. Polym. Sci.* **1991**, *43*, 817–823.
- (40) Crank, J. *The Mathematics of Diffusion*; Clarendon Press: Oxford, 1967.
- (41) Kim, J.; Reucroft, P.; Taghiei, M.; Pradhan, V.; Wender, I. *Prepr. Pap.—Am. Chem. Soc., Div. Fuel Chem.* **1992**, *37*, 756.
- (42) Rautenbach, R.; Mellis, R. Hybrid Processes Involving Membranes for the Treatment of Highly Organic/Inorganic Contaminated Waste Water. *Desalination* **1995**, *101*, 105–113.
- (43) Childress, A. E.; Elimelech, M. Effect of Solution Chemistry on the Surface Charge of Polymeric Reverse Osmosis and Nanofiltration Membranes. *J. Membr. Sci.* **1996**, *119*, 253–268.
- (44) Martin-Orue, C.; Bouhallab, S.; Garem, A. Nanofiltration of Amino Acid and Peptide Solutions: Mechanisms of Separation. *J. Membr. Sci.* **1998**, *142*, 225–233.
- (45) Forgach, D.; Rose, G.; Lutenske, N. Characterization of Composite Membranes by Their Non-equilibrium Thermodynamic Transport Parameters. *Desalination* **1991**, *80*, 275–292.

Received for review February 19, 1999  
Revised manuscript received July 9, 1999  
Accepted July 13, 1999

IE990140L